Atmos. Chem. Phys. Discuss., 12, 28343–28383, 2012
www.atmos-chem-phys-discuss.net/12/28343/2012/
doi:10.5194/acpd-12-28343-2012

Atmospheric Chemistry and Physics Discussions

Secondary organic aerosol formation from gasoline vehicle emissions in a new mobile environmental reaction chamber

S. M. Platt[1], I. El Haddad[1], A. A. Zardini[2], M. Clairotte[2], C. Astorga[2], R. Wolf[1], J. G. Slowik[1], B. Temime-Roussel[3], N. Marchand[3], I. Ježek[4], L. Drinovec[4], G. Močnik[4], O. Möhler[5], R. Richter[1], P. Barmet[1], F. Bianchi[1], U. Baltensperger[1], and A. S. H. Prévôt[1]

[1]Laboratory of Atmospheric Chemistry, Paul Scherrer Institute (PSI), Villigen, 5232, Switzerland
[2]Institute for Energy and transport, Sustainable Transport Unit, European Commission Joint Research Centre, 21027 Ispra, Italy
[3]Aix-Marseille Université, CNRS, LCE FRE 3416, 13331, Marseille, France
[4]Aerosol d.o.o., 1000 Ljubljana, Slovenia
[5]Institute for Meteorology and Climate Research, Karlsruhe Institute of Technology, 76021 Karlsruhe, Germany

Received: 21 September 2012 – Accepted: 1 October 2012 – Published: 26 October 2012

Correspondence to: A. S. H. Prévôt (andre.prevot@psi.ch)

Published by Copernicus Publications on behalf of the European Geosciences Union.

Abstract

We present a new mobile environmental reaction chamber for the simulation of the atmospheric aging of aerosols from different emissions sources without limitation from the instruments or facilities available at any single site. The chamber can be mounted on a trailer for transport to host facilities or for mobile measurements. Photochemistry is simulated using a set of 40 UV lights (total power 4 KW). Characterisation of the emission spectrum of these lights shows that atmospheric photochemistry can be accurately simulated over a range of temperatures from −7–25 °C. A photolysis rate of NO_2, J_{NO_2}, of $(8.0 \pm 0.7) \times 10^{-3}$ molecules cm^{-3} s^{-1} was determined at 25 °C. Further, we present the first application of the mobile chamber and demonstrate its utility by quantifying primary organic aerosol (POA) emission and secondary organic aerosol (SOA) production from a Euro 5 light duty gasoline vehicle. Exhaust emissions were sampled during the New European Driving Cycle (NEDC), the standard driving cycle for European regulatory purposes, and injected into the chamber. The relative concentrations of oxides of nitrogen (NO_x) and total hydrocarbon (THC) during the aging of emissions inside the chamber were controlled using an injection system developed as a part of the new mobile chamber set up. Total OA (POA + SOA) emission factors of $(370 \pm 18) \times 10^{-3}$ g kg^{-1} fuel, or $(14.6 \pm 0.8) \times 10^{-3}$ g km^{-1}, after aging, were calculated from concentrations measured inside the smog chamber during two experiments. The average SOA/POA ratio for the two experiments was 15.1, a much larger increase than has previously been seen for diesel vehicles, where smog chamber studies have found SOA/POA ratios of 1.3–1.7. Due to this SOA formation, carbonaceous particulate matter (PM) emissions from a gasoline vehicle may approach those of a diesel vehicle of the same class. Furthermore, with the advent of emission controls requiring the use of diesel particle filters, gasoline vehicle emissions could become a far larger source of ambient PM than diesel vehicles. Therefore this large increase in the PM mass of gasoline vehicle aerosol emissions due to SOA formation has significant implications

ACPD
12, 28343–28383, 2012

for our understanding of the contribution of on-road vehicles to ambient aerosols and merits further study.

1 Introduction

Airborne particulate matter (PM) damages health (Dockery et al., 1993; Dockery and Pope, 1994) and affects climate (IPCC, 2007). Environmental reaction chambers or *smog chambers* are of considerable utility in the study of PM (Hallquist et al., 2009 and references therein). One application of smog chambers is in the study of aerosol aging and the formation of secondary organic aerosol (SOA), which in the atmosphere constitutes a highly variable but significant fraction of the total aerosol mass (Hallquist et al., 2009). SOA is formed via the reactions of precursors, which may include materials already present in the condensed phase, but which partition at least to some extent to the gas phase (Donahue et al., 2006; Robinson et al., 2007). Thus any significant source of volatile organic compounds (VOCs) or primary, directly emitted, organic aerosol (POA) may be associated with the production of SOA, which when quantifying emissions, must be added to the POA emission. In this context large-scale combustion processes, such as biomass burning and fossil fuel combustion may be particularly important contributors to global SOA. Unfortunately SOA production has not been quantified for many important combustion sources.

In urban areas, where the health implications of pollutants are greater due to higher population density, road vehicles are an important source of PM (E.E.A., 2006), contributing for example, up to 50 % of the background aerosol mass in modern European cities (Mohr et al., 2011). Without considering SOA, diesel vehicles are the most significant contributor to urban vehicular PM, because diesel PM emission factors (EF) are orders of magnitude higher than those of gasoline vehicles and diesel vehicles constitute a large proportion of the European fleet. For example, based on a road-tunnel study, PM EFs of 3.4 vs. 0.16 g kg^{-1} fuel were observed for diesel and gasoline vehicles, respectively (Fraser et al., 2003). More recently, chassis dynamometer studies,

ACPD
12, 28343–28383, 2012

which offer the advantage of highly repeatable and controllable driving conditions, often following regulatory driving cycles (Barlow et al., 2009), have shown similar results, with primary PM EFs of 25.61 vs. 0.25 mg km^{-1} (total carbonaceous aerosol) for a Euro 4 diesel passenger car and a Euro 4 gasoline passenger car, respectively (Chirico et al., 2012). Furthermore, as mentioned above, a significant fraction of road traffic in Europe consists of diesel vehicles (veh). For example the Greenhouse Gas and Air Pollution Interactions and Synergies (GAINS) model, described in IIASA (2005), predicts that diesel light vehicles and heavy trucks accounted for an estimated 2200 G-veh km driven in the EU in 2010 vs. slightly fewer, 1820 G-veh km driven, for all gasoline vehicles excluding two-wheelers. Diesel vehicles are therefore subject to legislation aimed at reducing PM emission. For example the Euro 5 legislation for diesel passenger cars and the future Euro VI legislation for heavy duty diesel vehicles has necessitated the introduction of diesel particle filters (DPF) with close to 100 % mass efficiency (Johnson, 2008).

Emission inventories as well as vehicle legislation do not account for SOA production, the quantification of which from road vehicle emissions representative of those in the real world is technically challenging. Emission generation from high engine loads, i.e. at high speeds or during acceleration, when not done using on-road methodology (e.g. on board instrumentation or vehicle chasing), typically requires specialised testing facilities and the use of chassis dynamometers. Thus few smog chamber studies or estimates of SOA production and emission factors from vehicles exist, and so far only for diesel vehicles operated under steady state or simulated low power i.e. simultaneous application of power and brakes. Modest SOA production has been reported, e.g. 0.047 g kg^{-1} fuel, for a Euro 3 diesel passenger car at simulated 60 km h^{-1}, with a SOA/POA ratio of 1.3 (Chirico et al., 2010). Likely due to their low primary EFs, SOA production for gasoline vehicles has so far not been reported. This information is needed since without it, the relative importance of gasoline vehicles to PM pollution cannot be accurately estimated. Similarly, legislation designed to control vehicular PM may not be effective if only the primary aerosol is considered. Furthermore on a global

ACPD
12, 28343–28383, 2012

scale gasoline vehicles are more prominent than in Europe. Based on primary emissions only, bottom-up inventories using measured EFs, gasoline on-road vehicle emissions contribute 1029 Gg yr^{-1} to the global burden of primary carbonaceous aerosol, vs. 1084 Gg yr^{-1} from on-road diesel vehicles (Bond et al., 2004), despite lower per km PM emissions.

Measurements of SOA production are typically performed in smog chambers. However, the traditional, stationary, smog chamber is limited by the need to perform experiments with on-site instrumentation or aerosol sources. For ambient studies a further limitation is that only air in the immediate vicinity of the smog chamber may be sampled. The new Paul Scherrer Institute (PSI) mobile smog chamber was constructed to overcome these limitations by using a trailer mountable set up with a flexible, modular, design it is now possible to take the smog chamber to an emission source and make use of specialised testing facilities and instrumentation. Some features of this chmaber are similar to those of the mobile chamber used by Carnegie Mellon University (CMU), see e.g. Presto et al. (2011).

Here we characterise the mobile smog chamber in terms of its suitability for the simulation of atmospheric processes and demonstrate its utility by determining EFs for both POA and SOA production from a Euro 5 gasoline light duty vehicle during regulatory driving cycles on chassis dynamometers. These experiments required the transport to, installation, and operation of the chamber at a second facility, the Vehicle Emission Laboratory (VELA) of the the European Commission Joint Research Center (JRC), Italy.

2 Materials and methods

2.1 Mobile smog chamber and integrated systems

The mobile chamber and integrated systems, as set up during the gasoline vehicle emissions aging experiments are illustrated in Fig. 1, which also highlights the modular

ACPD
12, 28343–28383, 2012

design of the mobile smog chamber, while the instrumentation used in this study, is listed in Table 1. The modular design provides significant flexibility in terms of installation and operation at host facilities. For example during the gasoline vehicle emissions aging experiments, the chamber and sampling system was placed inside a testing cell with the vehicle, while the instruments and injection system were operated from outside of the cell. This allowed access to instrumentation during testing. Photographs illustrating this set up are shown in Fig. S1, in the Supplement (SI).

The mobile smog chamber (Fig. 1, purple) is an approximately 12 m^3 (when full), nominally 9 m^3 (2.5 × 1.8 × 1.9 m, L × W × H), 125 µm thick collapsible Teflon bag (DuPont Teflon fluorocarbon film (FEP), type 500A, Foiltec GmbH, Germany) suspended from a mobile aluminium frame (2.3 × 2 × 2.5 m, L × W × H) with a battery of 40 × 100 W UV lights (Cleo Performance solarium lamps, Philips).

Controlling concentrations of gas phase species (e.g. NO_x) inside smog chambers may be necessary in order to simulate atmospheric processes, see Sect. 2.3.2, therefore as illustrated in Fig. 2, the chamber is connected to an injection system, allowing the input of gases or liquids under controlled conditions. The injection system consists of a pure air generation system (Atlas Copco SF 1 Oil-free scroll compressor with 270 l container, Atlas Copco AG, Switzerland) with an air purifier (AADCO 250 series, AADCO Instruments, Inc., USA). The air from the pure air generation system has mixing ratios of oxygen (O_2) and nitrogen (N_2) matching that of ambient air while for other gas species the manufacturer's purity specifications include < 1 ppbv ozone (O_3), methane (CH_4) and non-methane hydrocarbons (NMHCs), nitrogen oxides (NO_x), hydrogen sulfide (H_2S), sulfur dioxide (SO_2), carbonyl sulfide (COS), carbon monoxide (CO), sulfur hexafluoride (SF_6), and fluorocarbons. Pure air may be injected directly into the chamber through the main injection line, an insulated 12 mm stainless steel tube which can be heated up to 150 °C (Fig. 2, red hatching, To Chamber). The maximum operational flow rate from the pure air generation system is 120 l min^{-1}. Since the Teflon bag is not fixed onto the frame, but rather suspended from rollers, the volume of the chamber may be adjusted by filling with pure air or withdrawing air through a pump.

ACPD
12, 28343–28383, 2012

Rapid cleaning of the chamber is therefore possible by sequentially reducing the bag volume to around 1 m^3 and flushing with O_3 and humidified, pure air (see Sect. 2.3.2).

All or part of the pure air stream may be diverted through different sections of the injection system using a series of two- and three-way valves. The ratio direct air into the main line to air through the injection system is controlled using rotameters. Gaseous components e.g. NO, NO_2, or propene (C_3H_6) are injected from gas bottles through one of two mass flow controllers: a low flow 1–1000 ml min^{-1} or a high flow 1–10 l min^{-1}. Air inside the chamber can be humidified by diverting part of the pure air at ~20 l min^{-1} through a glass flask containing heated ultrapure water. To prevent condensation, heated (~80 °C) stainless steel tubing (red hatching, Fig. 2) is used after the flask and the humidified stream is mixed with dry air in the main line, also heated to ~80 °C. O_3 is generated by passing pure air over a UV light source housed inside a stainless steel cylinder. Using this system O_3 concentrations in the range ppb – ppm can be generated inside the chamber. Nitrous acid (HONO) may be injected into the chamber using the continuous HONO generation system described by Taira and Kanda (1990). Briefly, constant flows of sodium nitrate and sulfuric acid, regulated by a programmable peristaltic pump (REGLO Digital MS-4/8, IDEX Health & Science GmbH, Germany), are mixed in a custom-built glass vessel to produce HONO. Pure air passes through the vessel to purge the HONO and then through a polytetrafluoroethylene (PTFE) filter before injection into the chamber. Waste chemical solution is removed from the vessel by the peristaltic pump. Liquid volatile organic compounds (VOCs) can be injected through a septum into the main injection line.

Emissions sampling into the chamber is performed using a modified ejector dilutor (DI-1000, Dekati Ltd, Finland), equipped with a pressurized air heater (DH-1723, Dekati Ltd, Finland). The Dekati is placed inside a stainless steel housing and may be heated up to 150 °C, preventing losses of emissions' hydrocarbons and aerosols. The sampling lines are constructed from separable 2 m segments of insulated 12 mm silica steel tubing (outer diameter), also heatable up to 150 °C. Using separable segments allows the distance between the chamber and emissions source to be varied as required,

ACPD
12, 28343–28383, 2012

providing maximum flexibility in terms of installation at different facilities. Sampling lines to the instrumentation are of variable length and constructed from stainless steel or copper for aerosol sampling, or Teflon for gas phase sampling. Temperature probes are placed at the top and the bottom surface of the bag (Fig. 1, T1 and T2). Relative humidity (RH) and a third temperature reading, are measured in the sampling lines directly adjacent to the chamber (Fig. 1, RH/T3).

Data from the gas phase instruments (NO_x, CO_2, total hydrocarbon (THC), O_3, Table 1 and Sect. 2.4) and the RH sensor are recorded and saved in real time using a data acquisition (DAQ) system (NI 9201 8 channel analogue input module and cDAQ-9178 8 slot USB chassis, National Instruments, Texas). Temperature at T1 and T2 is also recorded using the same DAQ system (NI 9214 16 channel module for high accuracy thermocouple measurements, National Instruments, Texas).

2.2 Light characterisation experiments

Actinometry experiments to determine the photolysis rate of NO_2 (J_{NO_2}) were performed to characterise the smog chamber lighting. 80 ppbv of nitrogen monoxide (NO, 1000 ppmv, 5.0, Carbagas) was injected into the chamber followed by injection of ozone (O_3). After allowing several minutes for equilibration the lights were switched on. NO_x and O_3 concentrations were monitored throughout (see Sect. 2.4.2 for details on smog chamber instrumentation). The photolysis of formaldehyde (HCHO) was also measured in a separate experiment, during which liquid HCHO (98 %, Aldrich) was injected into the chamber to produce a mixing ratio of 400 ppbv and shortly afterwards the UV lights were switched on. The HCHO concentration was monitored using a custom built absorption spectrometer based on the fluorimetric Hantzsch reaction, detailed in Belman (1963). Briefly, the reaction between acetyl acetone, ammonia and HCHO inside the instrument produces 3,5-diacetyl-1,4-dihydrolutidine, the fluorescence of which is proportional to the original HCHO concentration. HCHO reacts with OH radicals as well as undergoing photolysis. To account for this reaction, OH concentrations were measured using the "OH clock" methodology developed in Barmet et al. (2012). This

ACPD
12, 28343–28383, 2012

method involves spiking the chamber with 1 µl (~20 ppbv) of nine times deuterated butanol (butanol-D9, 98 % Aldrich), a unique OH tracer, and measuring its decay, here using a proton transfer reaction time of flight mass spectrometer (PTR-ToF-MS, Ionicon Analytik).

The light spectrum was measured using a photometer (USB2000 UVVIS, Ocean Optics, Inc., USA). The effect of varying temperature on light emission, and accordingly photochemistry, was inferred by placing a small number of UV lights inside a refrigeration unit and measuring the spectrum over the range −7 °C to 25 °C.

2.3 Gasoline exhaust aging experiments

We report the results of two emission aging experiments performed at the Vehicle Emission Laboratory (VELA) of the EC-JRC, on exhaust emissions from a gasoline light duty vehicle (GLDV). The experiments were conducted on 13 October 2011 (Exp. 1) and 14 October 2011 (Exp. 2). The emissions were studied after injection into the smog chamber and directly at the tail pipe. The emission measurements from the smog chamber also allowed an assessment of the performance of the smog chamber during typical operating conditions, including wall losses, leak rates and sampling efficiencies, see Sect. 3.1.

2.3.1 Vehicle emissions laboratory testing procedure

We studied the emissions of one EURO 5 GLDV on a chassis dynamometer (two 48" roller benches, Maha GmbH) climatic test cell (temperature range −10 °C to 35 °C) equipped with a constant volume sampler (CVS) with a critical flow venturi (Horiba, Germany).The temperature inside the test cell was 22 °C during the experiments. The GLDV features a three-way-catalyst (TWC) and stop-start system; technical details for this vehicle are summarised in Table S2.

Emissions were generated during the New European Driving Cycle (NEDC, Fig. 3, grey) used for type approval of light duty vehicles in Europe. The test started after a

ACPD
12, 28343–28383, 2012

mandatory minimum ambient temperature (22 °C) soaking time of 6 h and is made up of a first urban phase of 780s followed by an extra-urban phase of 400s, following EU Regulation 692/2008 (EC, 2008), as highlighted in Fig. 3. Regulated emissions (THC, NMHC, CO, NO_x, and PM) were sampled from the CVS and measured offline in accordance with Directive 70/220/EEC (EEC, 1970), and its following amendments by means of non-dispersive infrared (regulated CO and unregulated CO_2), chemiluminiscence (NO_x) and flame ionization detector (THC) (Horiba MEXA 7400 HTRLE). In addition, a time-resolved (1Hz) tailpipe emission characterisation was performed with the same methods described above (for CO, THC, NO_x and CO_2) and with a High Resolution Fourier Transform Infrared spectrometer (HR-FTIR, MKS Multigas analyzer 2030, Wilmington, MA, USA), used to monitor alkanes and alkenes (e.g. methane, ethylene and toluene), nitrogen species (NO_x and ammonia), and oxygenated compounds such as formaldehyde, acetaldehyde, and ethanol, see Clairotte et al. (2011) for details.

2.3.2 Smog chamber experimental procedure

Prior to all experiments the mobile chamber is cleaned by reducing its volume to $\sim 1\ m^3$ and flushing first with O_3 and humidified air, illuminating the chamber with UV light for a period of around 1 h and then flushing with pure dry air for several hours, typically overnight. At the start of each experiment the bag was filled to approximately two thirds full with humidified air (i.e. leaving a volume free for sample injection during several minutes). Emissions from the NEDC were then sampled directly at the vehicle tailpipe and injected into the chamber using the Dekati ejector dilutor. The Dekati and sampling lines were heated to 150 °C.

Subsequent to injection of the exhaust, the chamber was filled to close to maximum volume with pure air, ensuring more rapid mixing of the sample and allowing longer experiment times (since sampling from the chamber involves reducing its volume). To exclude partitioning induced artifacts due to higher than atmospherically relevant PM loadings, only enough of the total exhaust as was required to produce concentrations after injection of 30 and 15 µg of primary aerosol (representative of ambient PM

ACPD
12, 28343–28383, 2012

concentrations) in the chamber after final dilution, was injected during the first and second experiment, respectively. The relative humidity at this point was 50 % and 64 % for Exp. 1 and 2, respectively.

A period of several minutes was allowed for the equilibration inside the chamber and for characterisation of the primary emissions. After this 1 µl (∼ 20 ppbv) butanol-D9 was injected to quantify OH exposure during the experiment (see Sect. 2.2). Gasoline engines emit significant NO_x (Fig. 3) which consumes OH radicals, thereby altering the ozone production cycle and thus SOA formation, in a process dependent on the relative VOC concentration (Atkinson, 2000). Thus for these experiments ozone was injected to titrate NO to nitrogen dioxide (NO_2), to change from a reducing to an oxidising atmosphere, followed by propene (1000 ppm, 5.0, Carbagas) to adjust the ratio VOC/NO_x to, in the case of these experiments, approximately 6 : 1. The oxidation of propene is not likely to produce condensable products (due to its high volatility) and has previously been used to adjust the VOC/NO_x ratio during smog chamber experiments (Odum et al., 1996; Chirico et al., 2010). After adjusting the gases in the chamber and after allowing time for instrument readings of the injected gases to stabilise, the UV lights were switched on to initiate photochemistry. Aging of the emissions and associated SOA production were then measured during a period of ∼ 4 h.

The procedure described here may be adapted for the study of other emissions e.g. from ship engines, wood combustion etc. Adjustment of VOC/NO_x ratio, if at all necessary, may in other studies also be achieved by the addition of NO_x, in cases where the NO_x concentration is low in the chamber.

2.4 Instrumentation

Table 1 reports a non-exhaustive list of instrumentation typical of that available for measurements from the mobile chamber. Data from the high resolution time of flight aerosol mass spectrometer (HR-ToF-AMS) are analysed using high-resolution analysis fitting procedures. A detailed description of the working principles of the HR-ToF-AMS and associated data analysis may be found in DeCarlo et al. (2006). The HR-ToF-AMS used

ACPD
12, 28343–28383, 2012

for these experiments was equipped with a newly developed lens, which has a lower size limit of 100 nm for 100 % transmission, and can sample aerosol larger than 2.5 µm (Williams et al., 2012). Correcting scanning mobility particle sizer (SMPS) data from the chamber for density based on the relative contributions of sulphate, nitrate, ammonium and organics (assumed density 1.3 g cm^{-3}) measured by the HR-ToF-AMS, and subtracting black carbon (BC) as measured by the aethalometer, provides a second measurement of the total non-refractory PM mass (i.e. those species quantified in the HR-ToF-AMS). This second measure of non-refractory mass was used to correct for the collection efficiency (CE) of the HR-ToF-AMS.

BC concentrations and aerosol optical absorption spectra were measured using an Aethalometer (Model AE33 prototype). This new Aethalometer incorporates two parallel sampling channels from the same input stream collected at different rates of accumulation, resulting in different loading of the filter with collected aerosols on the two respective spots. Loading effects can then be extrapolated to zero, allowing online "loading effect" compensation for all wavelengths used for the measurement.

A suite of gas phase instruments was used here and is typically available for studies using the mobile smog chamber. Reactive gases such as O_3 and NO_x may be monitored throughout every experiment, while emphasis has also been placed on the measurement of combustion products, e.g. CO_2, CO, CH_4 and THC (Table 1). NO_x is monitored using instrumentation that measures directly NO as well as all nitrogen oxides (NO_y), with NO_y assumed to be almost exclusively NO_2 during most experiments.

A proton transfer reaction time-of-flight mass spectrometer (PTR-ToF-MS, Ionicon Analytik) was used to measure concentrations of VOCs inside the chamber, including that of butanol-D9. The instrument performances have already been described in detail previously (Jordan et al., 2009; Graus et al., 2010). The high mass resolution of the PTR-ToF-MS ($m/\Delta m$ ranging from 3200 to 4500 between m/z 21 and m/z 149) combined with an accuracy below 20 ppmv allows separation and formula assignment of most of the ions comprising the mass spectra of both primary and secondary vehicle emissions. Based on a 2 min integration time, typical LODs determined

ACPD
12, 28343–28383, 2012

as the 3σ uncertainty measured with a Pt catalyst heated at 350 °C were below 10 pptv. Data analysis was carried out using TOF Viewer 1.4.3. ToF-to-mass assignment was performed using hydronium ion isotope ($H_3^{18}O^+$, 21.022) and protonated acetone ($C_3H_7O^+$, 59.049). Peak fitting and integration was performed using Gaussian functions.

3 Results

3.1 Mobile chamber characterisation

The suite of tests conducted (see Sect. 2.2) and emission experiments (see Sect. 2.3) allowed us a detailed characterisation of the mobile chamber.

3.1.1 Chamber blank and leak rate

Figure 4 illustrates an example of results from the second emission experiment, showing time series and concentrations of several gas phase species as well as organic aerosol concentrations measured from the smog chamber and the temperature inside the chamber. In the empty chamber, before sample injection, measured particle number concentration was always below the CPC detection limit ($< 0.1\,cm^{-3}$), whereas the CO_2 concentration was around 35 ppmv. CO_2 did not increase during emissions aging (Fig. 4b, green), which would otherwise indicate significant leaks in the system. An average leak rate of $0.08\,\%\,h^{-1}$ (i.e. $\sim 9\,l\,h^{-1}$) was calculated by measuring the increase in CO_2 and CH_4 due to diffusion of external air into the empty chamber. The most likely source of these leaks is cracks in the chamber. These results show that the chamber has minimal contaminants and that leaks are minor over the course of a typical experiment lasting 5 to 6 h.

ACPD
12, 28343–28383, 2012

3.1.2 Temperature control

Since the chamber is not housed in an enclosure, the temperature inside the bag is that of the ambient. For the gasoline aging experiments the ventilation inside the VELA was sufficient to maintain a stable temperature to within 1 °C, as indicated in Fig. 4a.

3.1.3 Particle loss rates

During smog chamber experiments particles are lost to the walls through deposition following diffusion and gravitational settling. These losses limit the maximum duration of smog chamber experiments by continually removing suspended particle mass until instrument detection limits are reached. The loss rate for a given chamber depends largely on the surface to volume ratio of the chamber, with higher ratios leading to higher loss rates. Other parameters affecting particle loss rates include particle size (small particles have higher diffusion loss rates, while larger particles are more affected by gravitational settling) and turbulence inside the chamber, due to for example temperature gradients.

Aethalometer data, shown in Fig. S2 (SI), was used to determine particle loss rate to the chamber walls during the gasoline aging experiments based on the method adopted by Grieshop et al. (2009) and used in other combustion emission smog chamber studies (Chirico et al., 2010; Heringa et al., 2011). Briefly, by assuming an internally mixed aerosol, i.e. equal loss rate to the walls of all aerosol species, BC can be used to infer a wall loss corrected PM mass (PM_{WLC}):

$$PM_{WLC}(t) = \frac{PM(t)}{\exp(-t/t_{1/2})}, \quad (1)$$

where t and $t_{1/2}$ refer to experiment time and particle half-life, respectively. Although BC is expected to be inert, aethalometer measurements are affected by coating of soot particles with SOA, which increases the effective absorption coefficient and hence apparent concentration (Saathoff et al., 2003), clearly visible in Fig. S2. Therefore a

ACPD
12, 28343–28383, 2012

fitted BC concentration is used. Figure S2 also shows two such fits, one before lights on in the chamber, where no change in absorption from particle coating is expected, and one after 3 h of lights on where particle growth is negligible. The pre-UV exposure fit before lights on was chosen to correct for losses as the fit after lights is more likely to be influenced by coating. Significant influences due to turbulence during aging as a result of heating from the lights are not expected as only a small change in temperature after UV light exposure was observed and a longer half-life is observed during lights on (Fig. S2). Fitted BC data (Fig. S2) indicate a particle half-life due to wall losses of between 3.3 and 4.0 h for the period before lights on and the period after lights on, respectively, for Exp. 2. The particle half-life was shorter during Exp. 1, and the average half-life determined using fitted aethalometer data from the primary emissions (before lights on) over both experiments was 2.8 ± 0.8 h. These values indicate that particle losses in the chamber are sufficiently low to conduct experiments over several-hour timescales. Particle half-life in the mobile chamber is shorter than the average 5 h observed in the 27 m^3 PSI stationary smog chamber (Paulsen et al., 2005), an expected consequence of the increased surface to volume ratio of the mobile chamber.

3.1.4 Actinometry

Figure 5a shows the light spectrum at 25 °C (red) and −7 °C (blue) of the UV lights of the mobile smog chamber normalised to the peak intensity. The peak in emission is at 368 nm and is in a narrow window between 310–430 nm. The emission fingerprint as a function of wavelength and temperature, $(I(\lambda,T))$, of the smog chamber lighting overlaps with the absorption cross-section $(\sigma(\lambda,T))$ for the photolysis of many important atmospheric trace gases including the OH radical sources O_3, HONO, and HCHO, as well as NO_2 (DeMore et al., 1997; Atkinson et al., 2004, 2006). Therefore although emission intensity may be higher than sunlight over the spectral region at which they emit and much of the solar spectrum is not represented, UV lights are a good substitute for ambient sunlight in smog chambers (Carter, 1995). An advantage of UV lights over other light sources, such as for example xenon arc lights, is that they do not produce

ACPD
12, 28343–28383, 2012

significant heat. Consequently UV black lights are used in many environmental reaction chambers.

The photolysis rate of NO_2 (J_{NO_2}) can be calculated using the photostationary steady state relation:

$$[O_3] = \frac{J_{NO_2}[NO_2]}{k[NO]}, \quad (2)$$

where the concentrations of O_3, NO_2 and NO as well as the rate constant k between O_3 and NO are known (Seinfeld and Pandis, 2006), in this case from smog chamber measurements. NO_x was measured with both Thermo and Monitor labs NO_x analysers (Table 1) and an average J_{NO_2} of $(8.0 \pm 0.7) \times 10^{-3}$ molecules cm^{-3} s^{-1} was calculated from Eq. (2), after a correction of 5 % to account for formation of NO_2 in the (dark) sampling lines.

J_{NO_2} as a function of wavelength and temperature within a given window *λ2-λ1* is given by

$$J_{NO_2}(\lambda,T) = \int_{\lambda 1}^{\lambda 2} \varphi_{NO_2}(\lambda,T) \cdot \sigma_{NO_2}(\lambda,T) \cdot I(\lambda,T)\, d\lambda, \quad (3)$$

where $\varphi(\lambda,T)$ is the quantum yield of NO_2 photolysis as a function of wavelength and temperature (Seinfeld and Pandis, 2006). Thus while $I(\lambda,T)$ in Fig. 3a) is given by the light photometer in arbitrary units only, absolute values for the photolysis rates of a compound i (J_i) can be inferred from J_{NO_2}:

$$J_i = J_{NO_2} \cdot \frac{\int_{\lambda 1}^{\lambda 2} \varphi_i(\lambda,T) \cdot \sigma_i(\lambda,T) \cdot I(\lambda,T)\, d\lambda}{\int_{\lambda 1}^{\lambda 2} \varphi_{NO_2}(\lambda,T) \cdot \sigma_{NO_2}(\lambda,T) \cdot I(\lambda,T)\, d\lambda}. \quad (4)$$

Inferred photolysis rates at 25 °C from Eq. (4) are given for several compounds in Table 4, where International Union of Pure and Applied Chemistry (IUPAC) recommended

ACPD
12, 28343–28383, 2012

values of $\varphi(\lambda,T)$and $\sigma(\lambda,T)$ (Atkinson et al., 2006, 2004) were used in Eq. (4). The predicted photolysis rates show that the lighting system of the mobile smog chamber can be expected to be particularly effective in generating OH radicals from HONO or from HCHO (when in the presence of NO_x) and to a lesser extent from O_3.

Figure 5 shows that the emission fingerprint is largely unchanged over the given temperature range. Theoretical rate constants at −7 °C, shown in Table 4, were also determined using Eq. (4). The methodology for the calculation of $\varphi_{-7°C}(\lambda)$ and $\sigma_{-7°C}(\lambda)$ for each compound is given in the Supplement. For $I_{-7°C}(\lambda)$, measured values (Fig. 5a, blue) were used. Table 4 also shows the ratio of gas phase photolysis rates J_i at −7 °C and 25 °C, $J_{i,-7°C}/J_{i,25°C}$. The ratio is in the range 0.30–0.41, while the ratio in emission intensity at these temperatures, $I_{-7°C}(\lambda)/I_{-25°C}(\lambda)$, is 0.28 (Fig. 5b). Therefore the decrease in photolysis rates can be largely explained in terms of the decrease in emission intensity of the UV lights. A power fit (dashed lines Fig. 3b) of the measured intensity at different temperatures can therefore be used to predict the relative gas phase photolysis rate of species i as a function of temperature ($J_{\mathrm{rel},i}(T)$):

$$J_{\mathrm{rel},i}(T) = J_i(25°\mathrm{C}) \cdot \left(-0.064 \cdot \left(\frac{1.080}{1 + \exp(-2.466 - (T/6.218)} \right) \right). \quad (5)$$

Equation (5) suggests that although significant loss of intensity occurs at low temperatures, the lighting in the mobile chamber will still initiate photochemistry. The mobile chamber may thus be for aerosol aging studies even at zero or sub-zero temperatures. Under such conditions the HONO injection system described in Sect. 2.1 could be used to compensate for the loss in intensity by providing an additional OH source. As Fig. 5 illustrates the mobile chamber may be operated down to ∼10 °C without large loss in light intensity.

The predicted photolysis rate constants in Table 4 were validated using the decay in HCHO concentration measured in the mobile chamber under UV light. During the HCHO experiment OH was measured with a PTR-MS using the butanol-D9 tracer method. Note that the PTR-MS here is not the same instrument described in Sect. 2.4

ACPD
12, 28343–28383, 2012

used for the gasoline aging experiments. A predicted HCHO decay rate, including the sum of both photolysis pathways (at 25 °C) from Table 4 and OH reaction rates, $k_{OH+HCHO} = 8.5 \times 10^{-12}$ molecules cm^{-3} s^{-1} (Atkinson et al., 2006), is shown in Fig. S3 (SI). A background OH concentration of 3.6×10^6 cm^{-3} was calculated, with possible sources including HONO off-gassing from the chamber walls, previously suggested as a significant OH source in smog chambers (Metzger et al., 2008; Pfaffenberger et al., 2012), and photolysis of hydrogen peroxide (H_2O_2), a byproduct of HCHO photolysis. The rate constant k, determined from an exponential fit of measured data, and the predicted k was 9.5×10^5 molecules cm^{-3} s^{-1} and 8.3×10^5 molecules cm^{-3} s^{-1} respectively, indicative of small error only in the values given in Table 4.

During both aging experiments the OH exposure was close to zero molecules cm^{-3} h during sampling of primary emissions. The integrated exposure at the end of each experiment, after UV light exposure and aging, was around 11×10^6 molecules cm^{-3} (colour scale, Fig. 4). Assuming a global annual mean concentration of 10^6 OH molecules cm^{-3} h (Prinn et al., 2001), this corresponds to 11 h in the atmosphere, thereby demonstrating that the lighting of the chamber generates sufficient OH to study atmospheric processes occurring over relevant time scales.

While this study shows that the mobile chamber lighting can be used to simulate atmospheric photochemistry over a range of temperatures some uncertainties remain. For example the photolysis rates of some compounds, notably ketones and aldehydes, may be enhanced compared to ambient conditions when using UV lights (Carter, 1995). Furthermore oxidised SOA mass can be lost under UV black lights when OH concentration decreases from 10^7 to 10^6 molecules cm^{-3} s^{-1} (Donahue et al., 2012). This suggests that photolysis and other OA processing pathways initiated by the UV lights compete with the photooxidation pathways responsible for SOA formation. This effect would theoretically lead to an underestimation of the SOA production for the gasoline vehicle in this study, for example. However, the UV light and sunlight spectrums overlap, thus the relative importance of the SOA formation/ SOA processing

ACPD
12, 28343–28383, 2012

(likely photolysis) pathways will depend both on relative light intensity and OH concentrations, each highly variable in smog chambers and the ambient atmosphere.

3.2 Gasoline exhaust aging experiments

Figure 4 shows the concentrations measured with respect to time for several gas phase species as well as organic aerosol concentrations measured from the smog chamber during Exp. 2. Using this data, emissions factors for a pollutant P per mass of fuel combusted (EF_{MASS}), shown on the right axis for aerosol and hydrocarbon emissions as a function of time in Fig. 4, were calculated based on a carbon mass balance approach (adapted from Phuleria et al., 2006):

$$EF_{MASS} = \left(\frac{\Delta P}{\Delta C_{CO_2} + \Delta C_{CO} + \Delta C_{HC} + \Delta C_{OC} + \Delta C_{BC}} \right) \cdot W_C, \quad (6)$$

where C denotes carbon mass from CO_2, CO, gas phase hydrocarbon (HC), particle phase organic carbon (OC), from high resolution AMS analysis (Aiken et al., 2008) and black carbon (BC)). W_C is the fuel carbon mass fraction, 0.859, for the gasoline used. All values are determined from the change in concentration (Δ) observed in the smog chamber before and after sample injection or aging.

An emission factor per km (EF_{KM}) can then be calculated based on fuel economy:

$$EF_{KM} = EF_{MASS} \cdot e \cdot \rho, \quad (7)$$

Where e is the fuel economy, 5.27 and 5.22 l 100 km^{-1} for Exp. 1 and 2, respectively, and ρ is the fuel density, 0.759 kg l^{-1} for the gasoline fuel used.

3.2.1 Gas phase emissions

The average EFs over Exp. 1 and 2, where experimental conditions were the same, determined from smog chamber data using Eq. (6) and Eq. (7) for the Euro 5 GLDV

ACPD
12, 28343–28383, 2012

regulated compounds, CO, HC, non-methane hydrocarbons (NMHC) and NO_x, from the primary emissions as well as the Euro 5 limit values are shown in Table 2. HC and NMHC are reported in units of carbon mass, i.e. grams C kg^{-1} fuel. Figure 3 shows emissions of THC, CO and NO_x for Exp. 2 over the course of the NEDC.

As shown from the CVS data in Table 2, the GLDV in this study complies with Euro 5 regulations. Furthermore, emissions of regulated compounds are close to those previously observed from a Euro 5 GLDV during the NEDC cycle (EC, 2010 and Internal Communication, Joint Research Centre) as well as from a Euro 4 GLDV tested during different driving cycles (Chirico et al., 2012). This indicates that the vehicle of this study is typical of a modern, very clean gasoline passenger car as may be found on the road in Europe today. A substantial fraction of the VOCs in the primary emission, average 0.63 out of 0.84 g NMHC kg^{-1} fuel (carbon mass) over both experiments, could be identified and quantified using the PTR-ToF-MS.

Measurements of the THC concentration in the raw exhaust vs. those in the chamber could be also used to quantify VOC losses in the sampling system of the mobile chamber, Chirico et al. ()2010) suggest that SOA formation is unaffected by sampling line temperature over the range 80–150 °C, since an aerosol sample will respond dynamically to changes in temperature and concentration. That is, upon entering the smog chamber, emitted particles will partition as though in the atmosphere, regardless of temperature and concentration in the sampling system itself. However, SOA formation may also be influenced by the loss of gaseous precursors in the emission sampling lines. Assuming no loss of inert CO_2 in the system, the fraction of THC lost in the sampling lines can be estimated:

$$\text{THC lost} = 1 - \left(\frac{\Delta \text{THC}_{\text{Chamber}} / \overline{\text{THC}}_{\text{Exhaust}}}{\Delta \text{CO}_{2\text{Exhaust}} / \overline{\text{CO}}_{2\text{Exhaust}}} \right), \quad (8)$$

where $\Delta \text{THC}_{\text{Chamber}}$ and $\Delta CO_{2Chamber}$ is the change in THC and CO_2 concentration measured in the smog chamber, respectively, and $\overline{\text{THC}}_{\text{Exhaust}}$ and $\overline{\text{CO}}_{2\text{Exhaust}}$ are the

ACPD
12, 28343–28383, 2012

average exhaust concentrations of THC and CO_2 measured by VELA instrumentation. CO_2 in Eq. (8) can also be replaced with other tracers, such as NO, also measured from both smog chamber and using VELA instrumentation. Using this methodology an average THC loss of 20 % was determined, with both NO and CO_2 as tracers giving the same result. This calculated loss encompasses instrument error (two different instruments were used for each gas, one sampling from the chamber and one from the CVS), losses in instrument sampling lines, the effect of different measurement location (CVS in the VELA vs. smog chamber), losses to the chamber walls as well as losses in the exhaust sampling lines. Such losses appear minor, although depending on which individual VOCs, i.e. whether SOA precursors are lost, and to what extent, a small under-estimation of SOA production is possible.

For this study the emissions were sampled directly at the tailpipe of the vehicle, thereby avoiding potential particle losses in the CVS. The CVS operates with a dynamic dilution system, ensuring that the total flow through the system is constant, even as exhaust flow rate varies during a driving cycle. This offers significant advantages in terms of quantification, and indeed is required for legislative testing, but is likely to incur particle losses as the system is not heated even at relatively low dilution. In this study for example the dilution in the CVS varied between 2 and 200, while the average dilution during the whole NEDC for both experiments was 37, less than the dilution inside the chamber during both experiments (average dilution factor 100).

As Fig. 4a shows, a significant quantity of NO_x was present in the exhaust injected into the chamber during sampling, thereby requiring the addition of propene to produce atmospherically relevant OH concentrations inside the chamber, as described in Sect. 2.3.2. This is seen in the increase in THC concentrations in the smog chamber shortly before lights on, Fig. 4b, blue. The propene is likely to persist in the chamber after lights on, and oxidation products are also expected, thereby influencing many of the lighter aliphatic and oxygenated compounds, e.g. propene and formaldehyde, quantifiable using the PTR-ToF-MS. However, the added propene is unlikely to affect SOA measurements to a significant extent.

ACPD
12, 28343–28383, 2012

3.2.2 Particle phase emissions

Table 3 shows the two-experiment average EFs for carbonaceous aerosol from the GLDV. Black carbon (BC) emission factors were calculated using aethalometer data, presented in Fig. S2, from which average values $EF_{MASS} = (16.0 \pm 6) \times 10^{-3}$ g BC kg^{-1} fuel and $EF_{KM} = (0.6 \pm 0.2) \times 10^{-3}$ g BC km^{-1} were retrieved. A higher value, EF_{MASS} of 52.5×10^{-3} g BC kg^{-1} fuel is used in the emission inventory of Bond et al. (2004), for regions, e.g. United States and Europe, where relatively stringent emissions controls were in place as of 2004. This is consistent with the adoption of emissions controls and newer engine technology subsequent to 2004, e.g. Euro 4 in 2005 and Euro 5 in 2008. As expected, BC emissions for the GLDV were much lower than those observed for a diesel light duty vehicle (Chirico et al., 2010), Fig. 6, black. The Ångström exponent (α), a standardised parameter describing the decrease in light absorbance with respect to wavelength for BC, and a useful tool for source apportionment (Sandradewi et al., 2008) is also shown in Fig. S2 for Exp. 2. The initial value of 1.2 was obtained for aerosols from the gasoline car, which is higher than values reported for diesel cars (Sandradewi, 2008, and references therein). A slow reduction of α during the experiment was observed, except immediately after the UV-light switch-on, where a transient increase of α is observed. These changes could be caused by an increase of coating thickness due to condensation or evaporation, and oxidation of the adsorbed species.

As Fig. 6 shows, POA emissions from the GLDV are lower than those previously reported for a Euro 3 diesel vehicle equipped with an oxidation catalyst, but no DPF (Chirico et al., 2010). However, after aging of the emissions, SOA dominates OA for gasoline. The large increase in PM mass from gasoline car emissions due to SOA formation observed here, if it also occurs across a wider range of gasoline vehicles, would have very significant implications for our understanding of the contribution of gasoline vehicles to ambient PM. Furthermore, this SOA was formed after an OH exposure equivalent to approximately 11 h of ambient aging (assuming a 24-h ambient mean OH concentration of 10^6 cm^{-3}), indicating that SOA formation occurs rapidly in

ACPD
12, 28343–28383, 2012

the atmosphere. That is, significant gasoline vehicle SOA may be expected in the ambient atmosphere or around regions with large numbers of gasoline vehicles. This result is in agreement with a recent ambient study which concludes that gasoline SOA is the largest source of vehicular carbonaceous PM in the Los Angeles basin (Bahreini et al., 2012).

Indicated in the Fig. 4 is the O : C ratio of the POA and of the SOA, determined from the high resolution AMS analysis, which increases with time and OH exposure in the chamber. An increasing O : C, reflecting increasing oxygen content following oxidisation, is predicted by theory (Jimenez et al., 2009) and has been observed in ambient datasets (Ng et al., 2010). Highly aged ambient aerosols typically have O : C ratios approaching unity, whereas urban combustion related aerosol have been observed in the range 0.06–0.1 (Aiken et al., 2008). The O : C ratio of 0.7 observed here is the same as that of the ambient observed low volatility oxygenated organic aerosol (LV-OOA) (Ng et al., 2010). That is, the mobile smog chamber provides a good approximation of real atmospheric aging. The O : C ratio of smog chamber generated SOA aging has been linked to PM loading, with lower loadings resulting in higher O : C following increased partitioning of volatile species to the gas phase (Pfaffenberger et al., 2012). However, previous smog chamber studies, performed at similar PM concentrations to those here, on a wide range of emissions from wood burning (Heringa et al., 2011) to biogenic SOA precursors (Ng et al., 2010), do not typically result in the production of SOA with such high O : C (values below 0.5 are typically reported). This remarkable result suggests that the SOA precursors present in gasoline exhaust emissions become highly oxidised before condensing. The identity of these precursors is unknown and merits further study.

SOA represents only a modest mass fraction for the diesel vehicle shown in Fig. 6, green. The average factor increase in mass, after wall loss correction, was 15.1 and 1.3 for the gasoline and diesel vehicle, respectively. Similarly Robinson et al. (2007) report a factor of around 1.7 increase in mass due to aging (OH exposure 2×10^6 molecules cm^{-3}) from diesel emissions. This difference in emission profile after aging

ACPD
12, 28343–28383, 2012

may be largely explained in terms of differences in the magnitude of THC, i.e. SOA precursor, emissions, which are typically higher for modern gasoline than for diesel vehicles. The average THC emission from smog chamber data was 40 mg km^{-1}, while a value of 96.5 mg km^{-1} has also been reported for a Euro 5 GLDV from an NEDC cycle (EC, 2010). Diesel engines operate under lean conditions with a higher air/fuel ratio in comparison to the spark ignition engines typically used by GLDVs. For this reason, diesel engine exhaust contains less THC (as well as less CO and typically higher NO_x) than gasoline engine exhaust (Khair and Majewski, 2006).

SOA is not included in emissions inventories, (e.g. EEA, 2006; Bond et al., 2004), and would appear far less significant for diesel vehicles, especially those including an oxidation catalyst. That is, gasoline vehicles may be a significantly underestimated source of PM in urban areas. These results also suggest that the impact of diesel vehicles on ambient PM concentrations may further decrease in Europe where meeting emissions regulations will necessitate the use of DPFs on new vehicles. For example light duty diesel vehicles require a DPF in order to reach Euro 5 onwards, while heavy duty diesel vehicles are expected to require DPFs in order to meet Euro VI legislation (Johnson, 2008). The potential use of a particle filter for gasoline vehicles would likely be ineffective in reducing SOA as this is produced some time after emission from the tailpipe. A DPF has close to 100 % efficiency in terms of mass when used correctly. Thus most of the BC and POA shown in Fig. 6 for the diesel would be removed by fitting a DPF (though the effect of filter regeneration should not be neglected), leaving only the relatively small SOA fraction (Chirico et al., 2010), and total emissions would be much lower than those of the gasoline vehicle after aging. More studies, across a wider range of vehicles under different conditions are required.

4 Conclusions

We have shown that the new Paul Scherrer Institute mobile environmental reaction chamber can be of considerable utility in atmospheric science. Due to the flexible

ACPD
12, 28343–28383, 2012

design of the chamber, a wide range of emissions aging or ambient studies are possible with a single facility. We have demonstrated this utility and potential with results from measurements at a specialised testing facility, the Vehicle Emission Laboratory (VELA) of the European Commission Joint Research Center (JRC).

An understanding of the impact of vehicle emissions on public health and the environment requires an understanding of the sources of vehicular PM. We show that gasoline vehicle emissions can produce significant SOA. This suggests that the contribution of gasoline vehicles to ambient PM is considerably greater than previously thought. In contrast diesel vehicles produce much less SOA. Therefore these results suggest that both primary and secondary aerosol from vehicles should be included in PM models to realistically represent vehicle effects on ambient PM. However, this would require the development of a standardised protocol for determining the secondary aerosol production potential (SAPP). Since only one vehicle was tested, we suggest that SAPP from gasoline vehicles merits further study.

Supplementary material related to this article is available online at: http://www.atmos-chem-phys-discuss.net/12/28343/2012/acpd-12-28343-2012-supplement.pdf.

Acknowledgements. This work was supported by the Swiss Federal Office for the Environment (FOEN), the Federal Roads Office (FEDRO), The French Environment and Energy Management Agency (ADEME, Grant number 1162C00O2), EUROSTARS grant E!4825 FC Aeth and JR-KROP grant 3211-11-000519. Operation part-financed by the European Union, European Social Fund.

The VELA staff is acknowledged for its skilful technical assistance, in particular Franz Muehlberger, Urbano Manfredi, and Philippe Le Lijours.

We appreciate the insights into the details of the Carnegie Mellon mobile chamber and would like to thank the whole group of Allen Robinson and especially Albert Presto.

ACPD
12, 28343–28383, 2012

References

Aiken, A. C., DeCarlo, P. F., Kroll, J. H., Worsnop, D. R., Huffman, J. A., Docherty, K. S., Ulbrich, I. M., Mohr, C., Kimmel, J. R., Sueper, D., Sun, J. Y., Zhang, Q., Trimborn, A., Northway, M. J., Ziemann, P. J., Canagaratna, M., Onasch, T. B., Alfarra, M. R., Prevot, A. S. H., Dommen, J., Duplissy, J., Metzger, A., Baltensperger, U., and Jimenez, J. L.: O/C and OM/OC ratios of primary, secondary, and ambient organic aerosols with high-resolution time-of-flight aerosol mass spectrometry, Environ. Sci. Technol., 42, 4478–4485, 2008.

Atkinson, R.: Atmospheric chemistry of VOCs and NO_x, Atmos. Environ., 34, 2063–2101, 2000.

Atkinson, R., Baulch, D. L., Cox, R. A., Crowley, J. N., Hampson, R. F., Hynes, R. G., Jenkin, M. E., Rossi, M. J., and Troe, J.: Evaluated kinetic and photochemical data for atmospheric chemistry: Volume I – gas phase reactions of O_x, HO_x, NO_x and SO_x species, Atmos. Chem. Phys., 4, 1461–1738, doi:10.5194/acp-4-1461-2004, 2004.

Atkinson, R., Baulch, D. L., Cox, R. A., Crowley, J. N., Hampson, R. F., Hynes, R. G., Jenkin, M. E., Rossi, M. J., Troe, J., and IUPAC Subcommittee: Evaluated kinetic and photochemical data for atmospheric chemistry: Volume II – gas phase reactions of organic species, Atmos. Chem. Phys., 6, 3625–4055, doi:10.5194/acp-6-3625-2006, 2006.

Bahreini, R., Middlebrook, A. M., de Gouw, J. A., Warneke, C., Trainer, M., Brock, C. A., Stark, H., Brown, S. S., Dube, W. P., Gilman, J. B., and others: Gasoline emissions dominate over diesel in formation of secondary organic aerosol mass, Geophys. Res. Lett., 39, L06805, doi:10.1029/2011GL050718, 2012.

Barlow, T. J., Latham, S., McCrae, P. G., and Boulter, P. G.: A reference book of driving cycles for use in the measurement of road vehicle emissions (2009), United Kingdom Transport Research Laboratory (TRL), http://www.trl.co.uk/online_store/reports_publications/trl_reports/cat_traffic_and_the_environment/report_a_reference_book_of_driving_cycles_for_use_in_the_measurement_of_road_vehicle_emissions.htm (last access: May 2012), 2009.

Barmet, P., Dommen, J., DeCarlo, P. F., Tritscher, T., Praplan, A. P., Platt, S. M., Prévôt, A. S. H., Donahue, N. M., and Baltensperger, U.: OH clock determination by proton transfer reaction mass spectrometry at an environmental chamber, Atmos. Meas. Tech., 5, 647–656, doi:10.5194/amt-5-647-2012, 2012.

Belman, S.: The fluorimetric determination of formaldehyde, Anal. Chim. Acta, 29, 120–126, 1963.

ACPD
12, 28343–28383, 2012

Bond, T. C., Streets, D. G., Yarber, K. F., Nelson, S. M., Woo, J. H., and Klimont, Z.: A technology-based global inventory of black and organic carbon emissions from combustion, J. Geophys. Res. Lett., 109, D14203, doi:10.1029/2011GL050718, 2004.

Carter, W. P. L.: National Renewable Energy Laboratory (US), Environmental chamber studies of atmospheric reactivities of volatile organic compounds: Effects of varying chamber and light source, Statewide Air Pollution Research Center, 1995.

Chirico, R., DeCarlo, P. F., Heringa, M. F., Tritscher, T., Richter, R., Prévôt, A. S. H., Dommen, J., Weingartner, E., Wehrle, G., Gysel, M., Laborde, M., and Baltensperger, U.: Impact of aftertreatment devices on primary emissions and secondary organic aerosol formation potential from in-use diesel vehicles: results from smog chamber experiments, Atmos. Chem. Phys., 10, 11545–11563, doi:10.5194/acp-10-11545-2010, 2010.

Clairotte, M., Adam, T. W., Chirico, R., Giechaskiel, B., Manfredi, U., Elsasser, M., Sklorz, M., DeCarlo, P. F., Heringa, M. F., Zimmermann, R., Martini, G., krasenbrink, A., Vicet, A., Tournie, E., Prevot, A. S. H., and Astorga, C.: Online characterization of regulated and unregulated gaseous and particulate exhaust emission from two-stroke mopeds: a chemometric approach, Anal. Chim. Acta, 717, 28–38, doi:10.1029/2003JD003697, 2011.

DeCarlo, P. F., Kimmel, J. R., Trimborn, A., Northway, M. J., Jayne, J. T., Aiken, A. C., Gonin, M., Fuhrer, K., Horvath, T., Docherty, K. S., and others: Field-deployable, high-resolution, time-of-flight aerosol mass spectrometer, Anal. Chem., 78, 8281–8289, 2006.

DeMore, W. B., Sander, S. P., Golden, D. M., Hampson, R. F., Kurylo, M. J., Howard, C. J., Ravishankara, A. R., Kolb, C. E., Molina, M. J., and Jet Propulsion Lab, C. I. o. T. P.: Chemical kinetics and photochemical data for use in stratospheric modeling, Jet Propulsion Lab., California Inst. of Tech., Pasadena, CA, 1997.

Dockery, D. W. and Pope, C. A.: Acute respiratory effects of particulate air pollution, Annual Review of Public Health, 15, 107–132, 1994.

Dockery, D. W., Pope, C. A., Xu, X., Spengler, J. D., Ware, J. H., Fay, M. E., Ferris Jr., B. G., and Speizer, F. E.: An association between air pollution and mortality in six US cities, New England journal of medicine, 329, 1753–1759, 1993.

Donahue, N. M., Robinson, A. L., Stanier, C. O., and Pandis, S. N.: Coupled partitioning, dilution, and chemical aging of semivolatile organics, Environ. Sci. Technol., 40, 2635–2643, 2006.

Donahue, N. M., Henry, K. M., Mentel, T. F., Kiendler-Scharr, A., Spindler, C., Bohn, B., Brauers, T., Dorn, H. P., Fuchs, H., Tillmann, R., Wahner, A., Saathoff, H., Naumann, K.-H., Moehler,

ACPD
12, 28343–28383, 2012

O., Leisner, T., Mueller, L., Reinnig, M.-C., Hoffmann, T., Salo, K., Hallquist, M., Frosch, M., Bilde, M., Tritscher, T., Barmet, P., Praplan, A. P., DeCarlo, P. F., Dommen, J., Prevot, A. S. H., and Baltensperger, U.: Aging of Secondary Organic Aerosol via Gas-Phase OH Radical Reactions, P. Natl. Acad. Sci. USA, doi:10.1073/pnas.1115186109, 2012.

E.E.A.: EMEP/CORINAIR Emission Inventory Guidebook, European Environment Agency, http://www.eea.europa.eu/publications/emep-eea-emission-inventory-guidebook-2009 (last access: October 2012), Technical Report 11/2006, 2006.

EC: European Commission Regulation No 692/2008 of 18 July 2008 implementing and amending Regulation (EC) No 715/2007 of the European Parliament and of the Council on type-approval of motor vehicles with respect to emissions from light passenger and commercial vehicles (Euro 5 and Euro 6) and on access to vehicle repair and maintenance information, Official Journal of the European Communities, L199, 2008.

EC: Regulated emissions of a Euro 5 passenger car measured over different driving cycles, European Commission Joint Research Centre (JRC) Institute for Environment and Sustainability, http://www.unece.org/fileadmin/DAM/trans/doc/2010/wp29grpe/WLTP-DHC-04-03e.pdf (last access: July 2012), 2010.

EEA: EMEP/ CORINAIR Emission Inventory Guidebook, European Environment Agency, http://reports.ee.europa.eu/EMEPCORINAIR4 (last access: May 2012), Technical Report 11/2006, 2006.

EEC: The Council of the European Communities. Council Directive 70/220/EEC of 20 March 1970 on the approximation of the laws of the Member States relating to measures to be taken against air pollution by gases from positive-ignition engines of motor vehicles, Official Journal of the European Communities, L076, 1–22, 1970.

EPA: Environmental Protection Agency. Compendium of Methods for the Determination of Toxic Organic Compounds in Ambient Air, EPA method, EPA/625/R-96/010b, 1999.

Fraser, M. P., Buzcu, B., Yue, Z. W., McGaughey, G. R., Desai, N. R., Allen, D. T., Seila, R. L., Lonneman, W. A., and Harley, R. A.: Separation of fine particulate matter emitted from gasoline and diesel vehicles using chemical mass balancing techniques, Environ. Sci. Technol., 37, 3904–3909, 2003.

Graus, M., Müller, M., and Hansel, A.: High Resolution PTR-TOF: Quantification and Formula Confirmation of VOC in Real Time, J. Am. Soc. Mass Spectrom., 21, 1037–1044, 2010.

Grieshop, A. P., Logue, J. M., Donahue, N. M., and Robinson, A. L.: Laboratory investigation of photochemical oxidation of organic aerosol from wood fires 1: measurement and simulation

ACPD
12, 28343–28383, 2012

of organic aerosol evolution, Atmos. Chem. Phys., 9, 1263–1277, doi:10.5194/acp-9-1263-2009, 2009.

Hallquist, M., Wenger, J. C., Baltensperger, U., Rudich, Y., Simpson, D., Claeys, M., Dommen, J., Donahue, N. M., George, C., Goldstein, A. H., Hamilton, J. F., Herrmann, H., Hoffmann, T., Iinuma, Y., Jang, M., Jenkin, M. E., Jimenez, J. L., Kiendler-Scharr, A., Maenhaut, W., McFiggans, G., Mentel, Th. F., Monod, A., Prévôt, A. S. H., Seinfeld, J. H., Surratt, J. D., Szmigielski, R., and Wildt, J.: The formation, properties and impact of secondary organic aerosol: current and emerging issues, Atmos. Chem. Phys., 9, 5155–5236, doi:10.5194/acp-9-5155-2009, 2009.

Heringa, M. F., DeCarlo, P. F., Chirico, R., Tritscher, T., Dommen, J., Weingartner, E., Richter, R., Wehrle, G., Prévôt, A. S. H., and Baltensperger, U.: Investigations of primary and secondary particulate matter of different wood combustion appliances with a high-resolution time-of-flight aerosol mass spectrometer, Atmos. Chem. Phys., 11, 5945–5957, doi:10.5194/acp-11-5945-2011, 2011.

IIASA: The GAINS Model for Greenhouse Gases Version 1.0: Carbon Dioxide (CO_2), International Institute for Applied Systems Analysis, 2005.

IPCC: Contribution of Working Group I to the Fourth Assessment Report of the Intergovernmental Panel on Climate Change, ISBN 978-0-521-88009-1, Cambridge University Press, 2007.

Jimenez, J. L., Canagaratna, M. R., Donahue, N. M., Prevot, A. S. H., Zhang, Q., Kroll, J. H., DeCarlo, P. F., Allan, J. D., Coe, H., Ng, N. L., Aiken, A. C., Docherty, K. S., Ulbrich, I. M., Grieshop, A. P., Robinson, A. L., Duplissy, J., Smith, J. D., Wilson, K. R., Lanz, V. A., Hueglin, C., Sun, Y. L., Tian, J., Laaksonen, A., Raatikainen, T., Rautiainen, J., Vaattovaara, P., Ehn, M., Kulmala, M., Tomlinson, J. M., Collins, D. R., Cubison, M. J., Dunlea, E. J., Huffman, J. A., Onasch, T. B., Alfarra, M. R., Williams, P. I., Bower, K., Kondo, Y., Schneider, J., Drewnick, F., Borrmann, S., Weimer, S., Demerjian, K., Salcedo, D., Cottrell, L., Griffin, R., Takami, A., Miyoshi, T., Hatakeyama, S., Shimono, A., Sun, J. Y., Zhang, Y. M., Dzepina, K., Kimmel, J. R., Sueper, D., Jayne, J. T., Herndon, S. C., Trimborn, A. M., Williams, L. R., Wood, E. C., Middlebrook, A. M., Kolb, C. E., Baltensperger, U., and Worsnop, D. R.: Evolution of organic aerosols in the atmosphere, Science, 326, 1525, doi:10.1126/science.1180353, 2009.

Johnson, T. V.: Diesel emission control in review, SAE International Journal of Fuels and Lubricants, 1, 68–81, 2008.

ACPD
12, 28343–28383, 2012

Jordan, A., Haidacher, S., Hanel, G., Hartungen, E., L., M., Seehauser, H., Schottkowsky, R., Sulzer, P., and Märk, T. D.: A high resolution and high sensitivity proton-transfer-reaction time-of-flight mass spectrometer (PTR-TOF-MS), Int. J. Mass Spectrom., 286, 122–128, 2009.

Khair, M. K. and Majewski, W. A.: Diesel emissions and their control, Society of Automotive Engineers, 400 Commonwealth Dr, Warrendale, PA, 15096, USA, 2006.

Metzger, A., Dommen, J., Gaeggeler, K., Duplissy, J., Prevot, A. S. H., Kleffmann, J., Elshorbany, Y., Wisthaler, A., and Baltensperger, U.: Evaluation of 1,3,5-trimethylbenzene degradation in the detailed tropospheric chemistry mechanism, MCMv3.1, using environmental chamber data, Atmos. Chem. Phys., 8, 6453–6468, doi:10.5194/acp-8-6453-2008, 2008.

Mohr, C., DeCarlo, P. F., Heringa, M. F., Chirico, R., Slowik, J. G., Richter, R., Reche, C., Alastuey, A., Querol, X., Seco, R., Peñuelas, J., Jiménez, J. L., Crippa, M., Zimmermann, R., Baltensperger, U., and Prévôt, A. S. H.: Identification and quantification of organic aerosol from cooking and other sources in Barcelona using aerosol mass spectrometer data, Atmos. Chem. Phys., 12, 1649–1665, doi:10.5194/acp-12-1649-2012, 2012.

Ng, N. L., Canagaratna, M. R., Zhang, Q., Jimenez, J. L., Tian, J., Ulbrich, I. M., Kroll, J. H., Docherty, K. S., Chhabra, P. S., Bahreini, R., Murphy, S. M., Seinfeld, J. H., Hildebrandt, L., Donahue, N. M., DeCarlo, P. F., Lanz, V. A., Prévôt, A. S. H., Dinar, E., Rudich, Y., and Worsnop, D. R.: Organic aerosol components observed in Northern Hemispheric datasets from Aerosol Mass Spectrometry, Atmos. Chem. Phys., 10, 4625–4641, doi:10.5194/acp-10-4625-2010, 2010.

Odum, J. R., Hoffmann, T., Bowman, F., Collins, D., Flagan, R. C., and Seinfeld, J. H.: Gas/particle partitioning and secondary organic aerosol yields, Environ. Sci. Technol., 30, 2580–2585, 1996.

Paulsen, D., Dommen, J., Kalberer, M., Prévôt, A. S. H., Richter, R., Sax, M., Steinbacher, M., Weingartner, E., and Baltensperger, U.: Secondary organic aerosol formation by irradiation of 1, 3, 5-Trimethylbenzene-NO_x-H_2O in a New Reaction Chamber for Atmospheric Chemistry and Physics, Environ. Sci. Technol., 39, 2668–2678, 2005.

Pfaffenberger, L., Barmet, P., Slowik, J. G., Praplan, A. P., Dommen, J., Prévôt, A. S. H., and Baltensperger, U.: The link between organic aerosol mass loading and degree of oxygenation: an α-pinene photooxidation study, Atmos. Chem. Phys. Discuss., 12, 24735–24764, doi:10.5194/acpd-12-24735-2012, 2012.

ACPD
12, 28343–28383, 2012

Phuleria, H. C., Geller, M. D., Philip, M., and Sioutas, C.: Size-resolved emissions of organic tracers from light-and heavy-duty vehicles measured in a California roadway tunnel, Environ. Sci. Technol., 40, 4109–4118, 2006.

Presto, A. A., Nguyen, N. T., Ranjan, M., Reeder, A. J., Lipsky, E. M., Hennigan, C. J., Miracolo, M. A., Riemer, D. D., and Robinson, A. L.: Fine particle and organic vapor emissions from staged tests of an in-use aircraft engine, Atmos. Environ., 45, 3603–3612, 2011.

Prinn, R. G., Huang, J., Weiss, R. F., Cunnold, D. M., Fraser, P. J., Simmonds, P. G., McCulloch, A., Harth, C., Salameh, P., O'Doherty, S., and others: Evidence for substantial variations of atmospheric hydroxyl radicals in the past two decades, Science, 292, 1882–1888, 2001.

Robinson, A. L., Donahue, N. M., Shrivastava, M. K., Weitkamp, E. A., Sage, A. M., Grieshop, A. P., Lane, T. E., Pierce, J. R., and Pandis, S. N.: Rethinking organic aerosols: Semivolatile emissions and photochemical aging, Science, 315, 1259, doi:10.1126/science.1133061, 2007.

Saathoff, H., Naumann, K. H., Schnaiter, M., Schock, W., Mohler, O., Schurath, U., Weingartner, E., Gysel, M., and Baltensperger, U.: Coating of soot and $(NH_4)_2SO_4$ particles by ozonolysis products of [alpha]-pinene, J. Aerosol Sci., 34, 1297–1321, 2003.

Sandradewi, J., Prevot, A. S. H., Weingartner, E., Schmidhauser, R., Gysel, M., and Baltensperger, U.: A study of wood burning and traffic aerosols in an Alpine valley using a multi-wavelength Aethalometer, Atmos. Environ., 42, 101–112, 2008.

Seinfeld, J. H. and Pandis, S. N.: Atmospheric Chemistry and Physics, John Wiley and Sons Inc., New Jersey, 2006.

Taira, M. and Kanda, Y.: Continuous generation system for low-concentration gaseous nitrous acid, Anal. Chem., 62, 630–633, 1990.

Williams, L. R., Gonzalez, L., Peck, J., Trimborn, D., McInnis, J., Farrar, M., Moore, K., Jayne, J., Robinson, W., Lewis, D., Onasch, T., Canagaratna, M., Trimborn, A., Timko, M., Deng, R., Tang, D., de la Rosa Blanco, E., Prévôt, A. S. H., Smith, K., and Worsnop, D.: Design and characterization of an aerodynamic lens for transmitting particles >1 micrometer in diameter into the Aerodyne aerosol mass spectrometer, in preparation, 2012.

ACPD
12, 28343–28383, 2012

Table 1. Overview of instrumentation used to study the aging of emissions in the mobile smog chamber.

Measured Parameter	Instrument	Manufacturer	Lower limit/Range
Size resolved non-refractory particulate matter (mainly organics (OA), nitrates, sulfates, ammonia, chloride)	High Resolution Time-of-Flight Aerosol Mass Spectrometer (HR-ToF-AMS) with high pressure lens	Aerodyne	$< 1 \mu g\ m^{-3}/D_p$ 0.1–2.5 µm
Number-weighted aerosol size distribution	Scanning Mobility Particle Sizer (SMPS)	Home built, with TSI long DMA, TSI 3022 CPC	0.01 cm^{-3}, D_p 15–850 nm
Black carbon (BC)	Aethalometer AE33 (beta)	Aerosol d.o.o.	30 ng m^{-3} > 100 ng m^{-3} 10 ng m^{-3} > 100 µg m^{-3}
Particle number	Condensation particle counter CPC 3776	TSI	4 nm, 0.01–10^7 particles cm^{-3}
NO+NO_y (Trace level)	NO_x Monitor 42C	Thermo environmental	0–200 ppb
NO+NO_y	NO_x Monitor 9841A	Monitor Labs	0–2000 ppb
O_3	UV Photometric O_3 Analyzer Model 49C	Monitor Labs	0.05–1.0 ppm
CO_2+CO+CH_4+H_2O	Picarro Cavity Ring-Down Spectrometer G2401	Picarro	0–1000 ppm (CO_2) 0–5 ppm (CO) 0–20 ppm (CH_4) 0–7% (H_2O)
Total Hydrocarbon (THC)	THC Monitor APHA-370	Horiba	0.02–100 ppmC
Trace volatile organic compounds (VOCs)	Proton Time-of-Flight Mass Spectrometer (PTR-ToF)	Ionicon Analytik	10 ppt–1 ppm
Relative Humidity and temperature	Dew point hygrometer SC-05	Rotronic	RH 0–100 %, −40–100 °C
Temperature at smog chamber surface and sampling lines	Thermocouple type K	Messelemente Hettstedt	0–1200 °C

ACPD
12, 28343–28383, 2012

Table 2. Emission factors for regulated compounds calculated for a Euro 5 gasoline light duty vehicle from smog chamber data and VELA (CVS) data, averaged over two experiments, with the standard deviation, and Euro 5 limit values for gasoline light duty vehicles.

	CO	THC	NMHC	NO_x
From Smog Chamber Data				
EF_{MASS} (g kg^{-1} fuel)	13.76 ± 0.44	1.02 ± 0.08	0.84 ± 0.04	0.92 ± 0.22
EF_{KM} (g km^{-1})	0.55 ± 0.02	0.041 ± 0.003	0.034 ± 0.003	0.037 ± 0.009
From CVS Data				
EF_{MASS} (g kg^{-1} fuel)	18.84 ± 0.68	1.75 ± 0.21	1.75 ± 0.21	0.89 ± 0.14
EF_{KM} (g km^{-1})	0.741 ± 0.03	0.069 ± 0.009	0.069 ± 0.009	0.035 ± 0.005
Euro 5 Limit Values for GLDVs				
EF_{KM} (g km^{-1})	1.000	0.100	0.068	0.060

ACPD
12, 28343–28383, 2012

Table 3. Emission factors for carbonaceous aerosol for a Euro 5 gasoline light duty vehicle calculated from smog chamber data, averaged over two experiments with the standard deviation.

Emission factor (EF)	Black carbon (BC) $\times 10^{-3}$	Primary organic aerosol (POA) $\times 10^{-3}$	Secondary organic aerosol (SOA) $\times 10^{-3}$
EF_{MASS} (g kg^{-1} fuel)	16.0 ± 6.1	24.5 ± 19.7	345.4 ± 1.9
EF_{KM} (g km^{-1})	0.6 ± 0.2	1.0 ± 0.8	13.7 ± 0.0

ACPD
12, 28343–28383, 2012

Table 4. Predicted gas phase photolysis rates of selected compounds in the mobile smog chamber at 25 °C and −7 °C.

Compound	Reaction	J_i (10^{-5} cm^2 molecule^{-1} s^{-1})		Ratio
		25°C	−7°C	$J_{i,-7°C}/J_{i,25°C}$
Nitrogen dioxide	$NO_2 > NO+O(^3P)$	797	259	0.32
Ozone	$O_3 > O(^1D)$	43.1	17.8	0.41
Nitrous acid	$HONO > OH+NO$	214	68.4	0.32
Nitrate	$NO_3 > NO+O_2$	0.00	0.00	–
	$NO_3 > NO2+O(^3P)$	444	135	0.30
Formaldehyde	$HCHO > HCO+H$	1.50	0.53	0.36
	$HCHO > CO+H_2$	3.74	1.35	0.36
Acetaldehyde	$CH_3CHO >$ products	0.11	–	–
Methyl hydroperoxide.	$CH_3OOH >$ products	0.43	–	–
Glyoxal	$(CHO)_2 >$ products	0.71	–	–
Methyl vinyl ketone	$CH_3C(O)CH=CH_2 >$ products	0.34	–	–
Acetone	$CH_3C(O)CH_3 >$ products	0.01	–	–
Methyl nitrate	$CH_3ONO_2 >$ products	0.29	–	–
Peroxy acetyl nitrate (PAN)	$CH_3C(O)OONO_2 >$ products	0.04	–	–

ACPD
12, 28343–28383, 2012

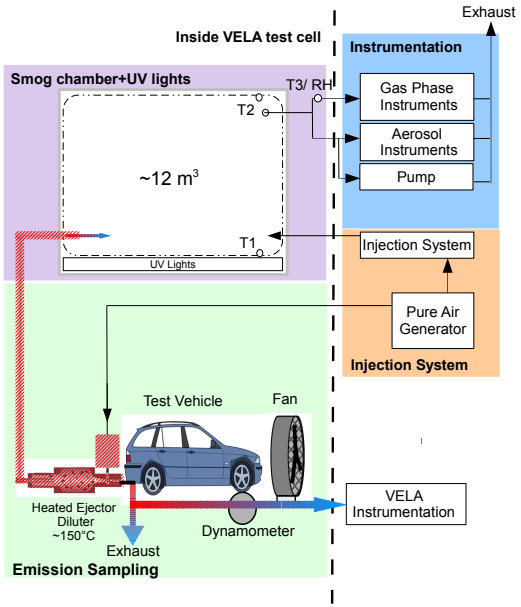

Fig. 1. Schematic (not to scale) of the mobile chamber as set up during experiments on a Euro 5 gasoline light duty vehicle emissions at the vehicle emissions laboratory (VELA) of the European Commission Joint Research Center (JRC), Ispra, Italy. Highlighted are different sections of the setup. Green: emissions sampling is performed using a modified Dekati ejector equipped with a pressurized air heater. Purple: the smog chamber. Blue: instrumentation, which was located outside of the test cell. Gas phase instruments are connected to the chamber via Teflon tubing, while steel or copper tubing is used to connect aerosol instruments.

ACPD
12, 28343–28383, 2012

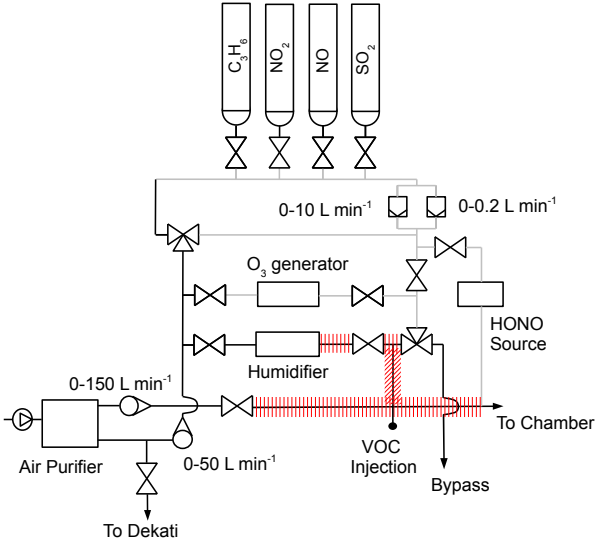

Fig. 2. Schematic (not to scale) of the primary component injection system of the mobile chamber. All or part of the pure air stream may be diverted through different sections of the primary injection system using a series of two- and three-way valves.

ACPD
12, 28343–28383, 2012

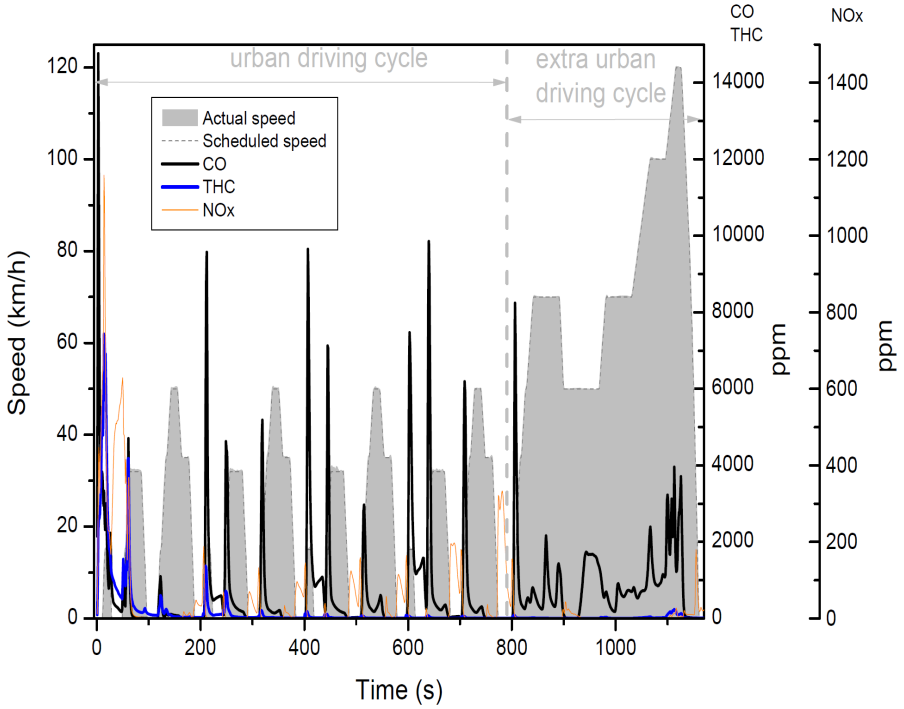

Fig. 3. Vehicle speed during the New European Driving Cycle (NEDC, grey area, left axis) and average exhuast concentrations of the regulated compounds carbon monoxide (CO, black) and total hydrocarbon (THC, blue), both on the first right axis, and oxides of nitrogen (NO_x, orange) second right axis, for Exp. 2 during the driving cycle. The NEDC is split into two phases representing urban driving and extra urban driving, respectively.

ACPD
12, 28343–28383, 2012

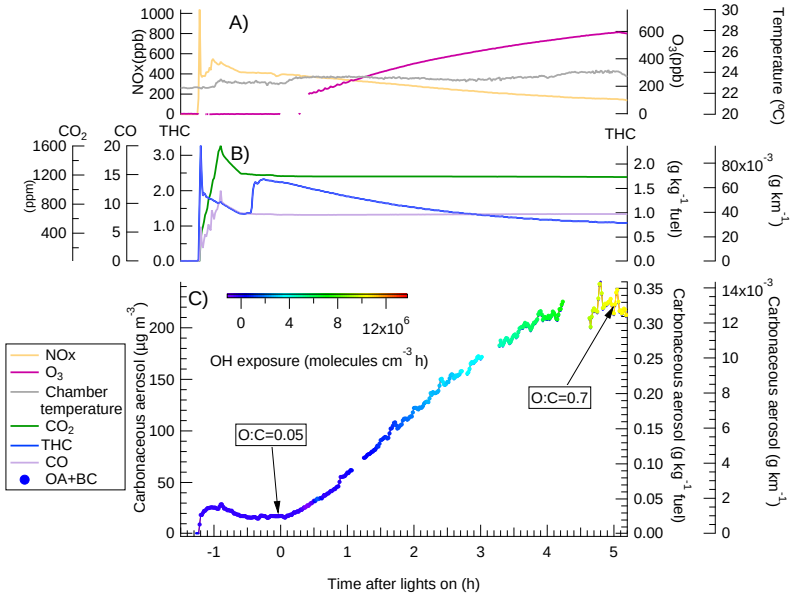

Fig. 4. Measured concentrations and calculated emissions factors (EF) inside the mobile smog chamber of gas and particle phase species after injection of emissions from a Euro 5 gasoline light duty vehicle (GLDV) (Exp. 2) as a function of time after lights on in the chamber. **(A)** NO_x (yellow), O_3 (magenta) and chamber temperature (grey). After an initial spike due to sample injection, a small decrease in NO_x before lights on follows the injection of additional air required to completely fill the chamber. O_3 increases after lights on as a consequence of the photochemical processing of emissions occurring inside the chamber. Temperature is stable to within 1 °C throughout the experiment. **(B)** Carbonaceous gases. After an initial decrease due to the dilution CO_2 (green) and CO (lilac) concentrations are constant indicating that the system is airtight. The increase in total hydrocarbon (blue) before lights on follows the addition of propene required to adjust the VOC/NO_x ratio. **(C)** Wall loss corrected carbonaceous aerosol (black carbon, BC + organic aerosol, OA) increases after lights on due to secondary organic aerosol (SOA) formation. OH exposure is shown by the colour scale. Aging increases the O : C ratio of the emissions from 0.05 for the primary to 0.7 for the secondary, a ratio equivalent to the low volatility oxidised OA observed in highly aged ambient aerosols. The right axis in **(B)** and **(C)** shows the EF calculated for THC and carbonaceous aerosol using Eqs. (6) and (7).

ACPD
12, 28343–28383, 2012

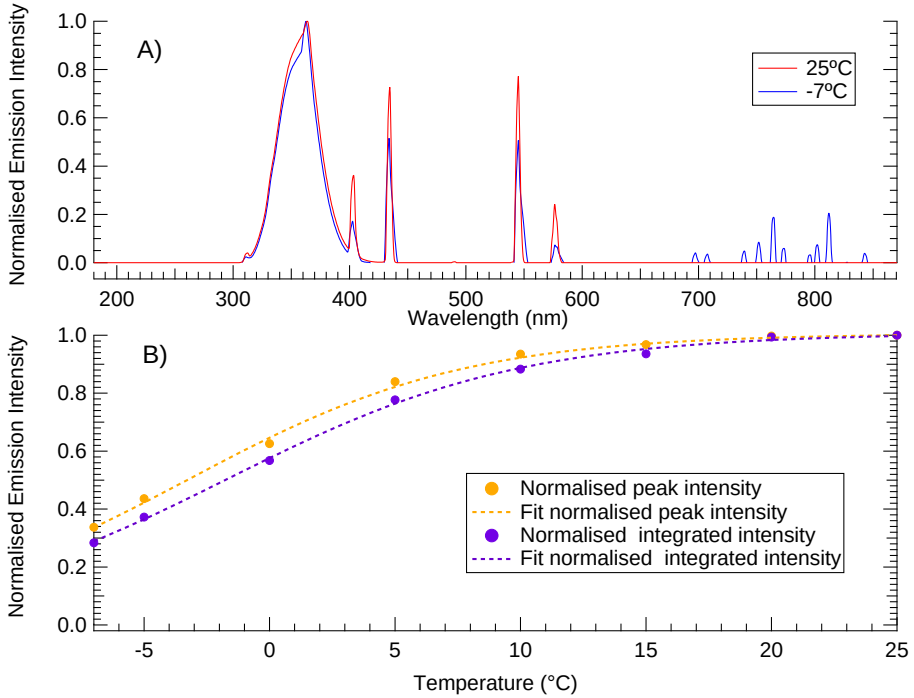

Fig. 5. (A) Emission spectrum of the UV black lights of the mobile smog chamber normalised to the peak in emission at 368 nm at 25 °C (red) and −7 °C (blue). The emission fingerprint does not change significantly over this temperature range. **(B)** The normalised intensity of the smog chamber lighting measured at 368 nm and from integrating the full spectrum. The dashed lines show a power fit to the data. Intensity does not vary significantly between 10 °C and 25 °C (less than ∼ 10 % decrease). At −7 °C, intensity is decreased significantly (∼ 70 % decrease).

ACPD
12, 28343–28383, 2012

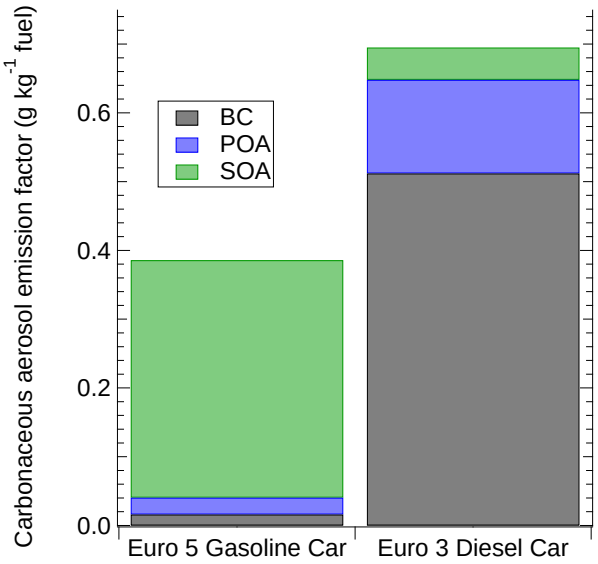

Fig. 6. Aerosol emission factors calculated for the Euro 5 gasoline light duty vehicle (GLDV) (average over Exp. 1 and 2) of this study and the results of a previous smog chamber study on a Euro 3 diesel passenger car (with oxidation catalyst, but without diesel particle filter, DPF) by Chirico et al. (2010). The diesel emissions are dominated by black carbon (BC, black) and primary organic aerosol (POA, blue) with only a small secondary organic aerosol (SOA, green) fraction. Conversely, a large fraction of the GLDV emission comprises SOA after aging. The large SOA fraction for the GLDV suggests a larger contribution from gasoline vehicles to ambient particulate pollution than has so far been recognised based on primary emissions. Further, future use of DPFs would remove almost all of the primary BC and POA emissions from diesel vehicle emissions, in which case the total particulate emissions (i.e. POA + SOA) for the GLDV may exceed those of a diesel vehicle.

ACPD
12, 28343–28383, 2012